ELSEVIER

Materials Science and Engineering A 441 (2006) 1–17

MATERIALS SCIENCE & ENGINEERING A

www.elsevier.com/locate/msea

Review

Overview of processing, microstructure and mechanical properties of ultrafine grained bcc steels

R. Song [a,*], D. Ponge [b], D. Raabe [b,**], J.G. Speer [a], D.K. Matlock [a]

[a] *Department of Metallurgical and Materials Engineering, Colorado School of Mines, Golden, CO 80401, USA*
[b] *Max-Planck-Institut für Eisenforschung, Max-Planck-Str. 1, 40237 Düsseldorf, Germany*

Received 18 July 2006; received in revised form 3 August 2006; accepted 25 August 2006

Abstract

Ultrafine grained steels with grain sizes below about 1 μm offer the prospect of high strength and high toughness with traditional steel compositions. These materials are currently the subject of extensive research efforts worldwide. Ultrafine grained steels can be produced either by advanced thermomechanical processes or by severe plastic deformation strategies. Both approaches are suited to produce submicron grain structures with attractive mechanical properties. This overview describes the various techniques to fabricate ultrafine grained bcc steels, the corresponding microstructures, and the resulting spectrum of mechanical properties.

Keywords: Ultrafine grained steels; Microstructure; Thermomechanical processing; Severe plastic deformation; Mechanical properties

Contents

* Corresponding author. Tel.: +1 303 273 3624; fax: +1 303 273 3016.
** Corresponding author. Tel.: +49 211 6792 340.
E-mail addresses: rsong@mines.edu (R. Song), d.raabe@mpie.de (D. Raabe).

0921-5093/$ – see front matter © 2006 Elsevier B.V. All rights reserved.
doi:10.1016/j.msea.2006.08.095

1. Introduction

Among the different strengthening mechanisms, grain refinement is the only method to improve both strength and toughness simultaneously. Therefore, ultrafine grained steels with relatively simple chemical compositions, strengthened primarily by grain refinement, have great potential for replacing some conventional low alloyed high strength steels. The main benefits behind such an approach are to avoid additional alloying elements; to avoid additional heat treatments like soft annealing, quenching and tempering; and to improve weldability owing to lower required carbon contents and other alloying elements when compared with other high strength steels. A further high potential domain for such ultrafine grained steel is the possibility for high strain rate superplasticity at medium and elevated temperatures [1]. In general, the term ultrafine grain is used here in the context of average grain sizes between 1 and 2 μm in diameter; submicron refers to grain sizes between 100 and 1000 nm; while nanostructured refers to grain sizes below about 100 nm.

The purpose of this overview is to provide a detailed introduction to the processing technologies, to the resulting microstructures, and to the mechanical properties associated with ultrafine grained body centered cubic (bcc) steels.

2. Methods of producing ultrafine grained steels

2.1. Introduction

Currently, laboratory techniques to produce ultrafine grained bcc steels utilize two approaches: severe plastic deformation techniques or advanced thermomechanical processing, which essentially involves modification to conventional large scale steel rolling processes. Compared to severe plastic deformation techniques, advanced thermomechanical methods are large-scale industrial processes and can be somewhat more readily optimized to operate in temperature regimes where they beneficially exploit phase transformation and controlled cooling.

2.2. Severe plastic deformation

2.2.1. Severe plastic deformation techniques for steels

Severe plastic deformation (SPD) techniques [2–4] impose large accumulated plastic strains at room or elevated temperatures, e.g. mainly in the temperature regime of warm deformation. These techniques can be used to produce ultrafine grained steels with an average grain size below 1 μm [5–19]. Typical SPD techniques include equal-channel angular pressing (ECAP) [5–11], accumulative roll bonding (ARB) [12–14], bi-directional compression [15], and high-pressure torsion (HPT) [16–19].

2.2.2. Equal-channel angular pressing

Equal-channel angular pressing imposes large plastic strains on massive billets via a pure shear strain state. The approach was developed by Segal et al. in the early 1980s [20]. Its goal was to introduce intense plastic strain into materials without changing the cross-sectional area of the deformed billets. Owing to this characteristic, repeated deformation is possible. At the beginning of the 1990s this method was further developed and applied as a severe plastic deformation method for the processing

of microstructures with submicron grain sizes [21]. The equal-channel angular pressing method was mainly applied for non-ferrous alloys (e.g. Al and Mg alloys) and some low carbon steels. The finest ferrite grain size obtained by use of this method is reportedly about 0.2 μm [7,22].

2.2.3. Accumulative roll bonding

Accumulative roll bonding essentially involves repeated application of conventional rolling. This approach has been suggested to possess the potential for mass production [12–14,23–25]. While rolling is an attractive deformation process for continuous production of bulk sheets, the total reduction in thickness, i.e. the accumulated strain, which can be achieved by this method, is limited because of the decrease in the strip thickness with increasing rolling reduction. In order to obtain bulk material, rolled sheets are stacked and then bonded together during rolling. Hence, the process involves simultaneous bonding and deformation. In the accumulative roll bonding method, the rolled material is cut, stacked to the initial thickness and rolled again. Owing to this approach, multiple repetitions are possible to achieve huge strains. A natural limit of this approach lies in the increase in strength and the gradually reduced surface quality of the roll-bonded sheets.

2.2.4. High pressure torsion

High-pressure torsion (HPT) imposes a pressure of up to several GPa for the fabrication of disk shaped samples with a diameter from 10 to 20 mm and a thickness of 0.2–0.5 mm [19]. A disk shaped specimen, which is usually first provided as a powder sample, is compressed in an almost closed die. During loading, the contact platens rotate in opposite directions in order to impose a shear strain. The through-thickness distribution of shear strain depends on the contact friction, a function of the roughness of the contact plates and the lubrication state. The torsion straining achieves a substantial degree of substructure refinement and controls the evolution of large crystallographic misorientations among adjacent grains. The HPT technique also has the advantage of being able to refine the grain size during powder consolidation, making it possible to produce bulk nanomaterials from micrometer-sized metallic powders.

2.2.5. Bi-directional large strain deformation

Bi-directional compression can be used to introduce large plastic strains in steels. It combines severe plastic deformation (large strain) and thermomechanical processing (phase transformation and controlled cooling can be exploited). Compression is realized by alternate forging in two perpendicular directions. Elongation in the third direction is usually not restricted.

2.3. Advanced thermomechanical processes

2.3.1. Introduction

In contrast to severe plastic deformation approaches in which large strain is the main factor, advanced thermomechanical processes pursue alternative strategies to produce ultrafine ferrite grains. For instance, these processes exploit dynamic recrystallization of austenite during hot deformation with subsequent $\gamma \rightarrow \alpha$ (austenite to ferrite) transformation [26]; strain-induced ferrite transformation (i.e. transformation during rather than after deformation) [27–32]; hot rolling in the intercritical region (i.e. in the austenite/ferrite two-phase region) [33]; warm rolling in the ferrite region [34] involving either dynamic recrystallization or pronounced recovery of the ferrite during warm deformation [35–45]; or cold rolling and annealing of a martensitic starting microstructure [46–51].

2.3.2. Recrystallization of austenite during hot deformation

An important mechanism that is widely used for grain refinement in steels is dynamic recrystallization during hot deformation [26]. This technique has been used to produce ferrite grain sizes as fine as 2–5 μm via recrystallization-controlled rolling or by conventional rolling followed by accelerated cooling. In recrystallization-controlled rolling fine precipitates restrict austenite grain growth after deformation. Recrystallization-controlled rolling is often used in conjunction with accelerated cooling and microalloying in order to effectively refine the grain size. Accelerated cooling is used to increase the cooling rate through the transformation zone in order to decrease the transformation temperature. In principle, a lower transformation temperature results in a higher ferrite nucleation rate due to a higher undercooling, and a decreased growth rate. Conventional controlled rolling has been implemented in many commercial operations through the addition of elements such as Nb, which increases the recrystallization temperature to over 1173 K, such that deformation in the last passes are applied below the recrystallization temperature. This increases the density of sites for ferrite nucleation.

2.3.3. Strain-induced ferrite transformation

A simple rolling procedure which entails strain-induced phase transformation from austenite to ferrite has been found to provide significant grain refinement in the sheet surface. In this approach, steel strips are reheated to obtain austenite microstructure and subsequently rolled in a single pass (30% reduction) just above A_{r3} (austenite to ferrite transformation temperature) but below A_{e3} (equilibrium austenite to ferrite transformation temperature) [27,52–56]. The three critical factors promoting the formation of ultrafine ferrite grains during a strain-induced transformation are a high shear strain, a high cooling rate as a result of rapid heat transfer to the colder rolls during the roll pass, and an appropriate deformation temperature (between A_{r3} and A_{e3}).

Hodgson et al. [27] applied strain-induced transformation to a plain carbon steel strip (0.06C–0.59Mn, wt.%) with an original thickness of about 2 mm, reduced to about 1.4 mm after a single pass at roll exit temperatures between 953 and 983 K. Equiaxed ultrafine ferrite grains of about 1 μm in the subsurface region were obtained, but the microstructure of the rolled strip was inhomogeneous through the thickness. The microstructure consisted of ultrafine ferrite grains in the surface layers, which penetrated to between one-quarter and one-third of the thickness with coarser ferrite (about 5–10 μm) and pearlite in the core of the strip.

2.3.4. Intercritical hot rolling

Ultrafine ferrite grains in plain C–Mn steels have also been obtained through hot rolling in the intercritical region (i.e. in the austenite plus ferrite two-phase region) by Yada et al. [57]. They attributed grain refinement to both dynamic transformation of austenite into ferrite and the dynamic recrystallization of the ferrite phase. Nucleation of ferrite at austenite grain boundaries during the dynamic transformation was considered to play a major role in the formation of ultrafine ferrite grains while dynamic recrystallization of ferrite was assumed to be of minor relevance.

2.3.5. Dynamic recrystallization of ferrite during warm deformation

Warm deformation in the ferrite regime may further refine steel microstructures that were previously refined during transformation. It has been considered that recovery is the main softening process during warm deformation of ferrite and that dynamic recrystallization does not occur [35]. This behavior is attributed to the fact that bcc ferrite has a high stacking fault energy which results in rapid recovery and insufficient accumulation of stored deformation energy to promote dynamic recrystallization. However, the occurrence of dynamic recrystallization of ferrite has been reported by several researchers [35–37,58]. The recent study of Murty et al. [36] confirmed the occurrence of dynamic recrystallization of ferrite in an ultra-low carbon steel processed by warm deformation at a strain rate of 0.01 s^{-1} (low Zener–Hollomon parameter). Since warm deformed ferrite usually contains pronounced subgrain structures that are sometimes difficult to distinguish from recrystallized grains in standard light optical micrographs, the authors confirmed the occurrence of dynamic recrystallization in ferrite by use of the electron backscattered diffraction (EBSD) technique to characterize the crystallographic relationships across grain boundaries. Most of the equiaxed ferrite grains were surrounded by high-angle grain boundaries (HAGBs) (with grain boundary misorientations $\geq 15^\circ$) rather than by low-angle grain boundaries (with grain boundary misorientations $<15^\circ$).

In another case, warm-rolling of interstitial free (IF) steel in the ferrite region was found by Najafi-Zadeh et al. [34] to produce ultrafine ferrite with grain size of 1.3 μm. Dynamic recrystallization of ferrite was considered to play a major role in the formation of ultrafine ferrite. A key barrier to the occurrence of dynamic recrystallization of ferrite is suggested to involve the presence of interstitial elements such as C and N. Removing interstitial elements from the matrix reduces the possibility of strain-induced precipitation, which inhibits dynamic recrystallization and increases the likelihood of dynamic recrystallization of ferrite [34].

2.3.6. Pronounced recovery of ferrite during warm deformation and annealing

Recently, Song et al. [39–45] have reported the production of ultrafine ferrite through pronounced recovery following warm deformation and annealing. Compared with the earlier studies on low carbon ultrafine grained bcc steels, Song et al. [39–45] investigated medium carbon steels in an effort to increase the work hardening rate of ultrafine grained steels, since high work hardening rates are associated with high ductility. In their studies, steels with ultrafine ferrite grains and homogeneously distributed cementite particles were produced by large strain warm deformation ($\varepsilon = 1.6$) at 823 K and subsequent annealing (Fig. 1). The ultrafine microstructures obtained were stable against grain and cementite coarsening even during a 2 h annealing treatment at 823 K. Pronounced recovery instead of primary recrystallization was required to obtain a large fraction of HAGBs. It was concluded in [39] that the prevalence of primary recrystallization, instead of recovery, is not generally beneficial in warm rolling. Primary recrystallization reduces significantly the dislocation density and removes the substructure, which is important for the gradual formation of subgrains that eventually become ultrafine grains surrounded by HAGBs.

2.3.7. Cold rolling and annealing of martensitic steel

Another route to fabricate ultrafine grained steel was developed by Tsuji et al. [49–51]. The process includes cold-rolling (50% reduction) of a martensite starting microstructure in a low carbon steel (0.13 wt.% C) and subsequent annealing at 773–873 K. The final microstructure was reported to consist of ultrafine ferrite grains and uniformly precipitated carbides. The formation of an ultrafine microstructure was attributed to the fine martensite starting microstructure, which augmented the effect of plastic deformation enhancing grain subdivision [49–51]. The high dislocation density as a result of cold rolling and the high concentration of solute carbon atoms in the martensite were also expected to facilitate grain subdivision by causing inhomogeneous deformation [49–51].

2.4. Summary of the two strategies of producing ultrafine grained steels

2.4.1. Differences

As mentioned above, ultrafine grained steels can be produced by two main methods. Table 1 gives a summary of the various process techniques described above and the ferrite grain sizes obtained for the different bcc steels. Among the SPD techniques the accumulated plastic strains (true strains) required to obtain submicron-sized grains are of the order of 3–4 using ECAP and of the order of 5–6 using the ARB process. For the SPD methods, a well-designed strain path is more important and also more feasible than a precisely controlled temperature path. The small-scale complexity and the "batch" nature of these methods suggest that they would require considerable ingenuity and investment for application to high volume steel production.

The advanced thermomechanical processing routes employ a relatively low accumulated strain in the range of about 1.0–3.6 to produce ultrafine grained steels (except for the strain-induced ferrite transformation technique which typically requires even less strain). The advanced thermomechanical processing methods are less effective with respect to grain refinement, but more adaptable to large sample sizes when compared with the

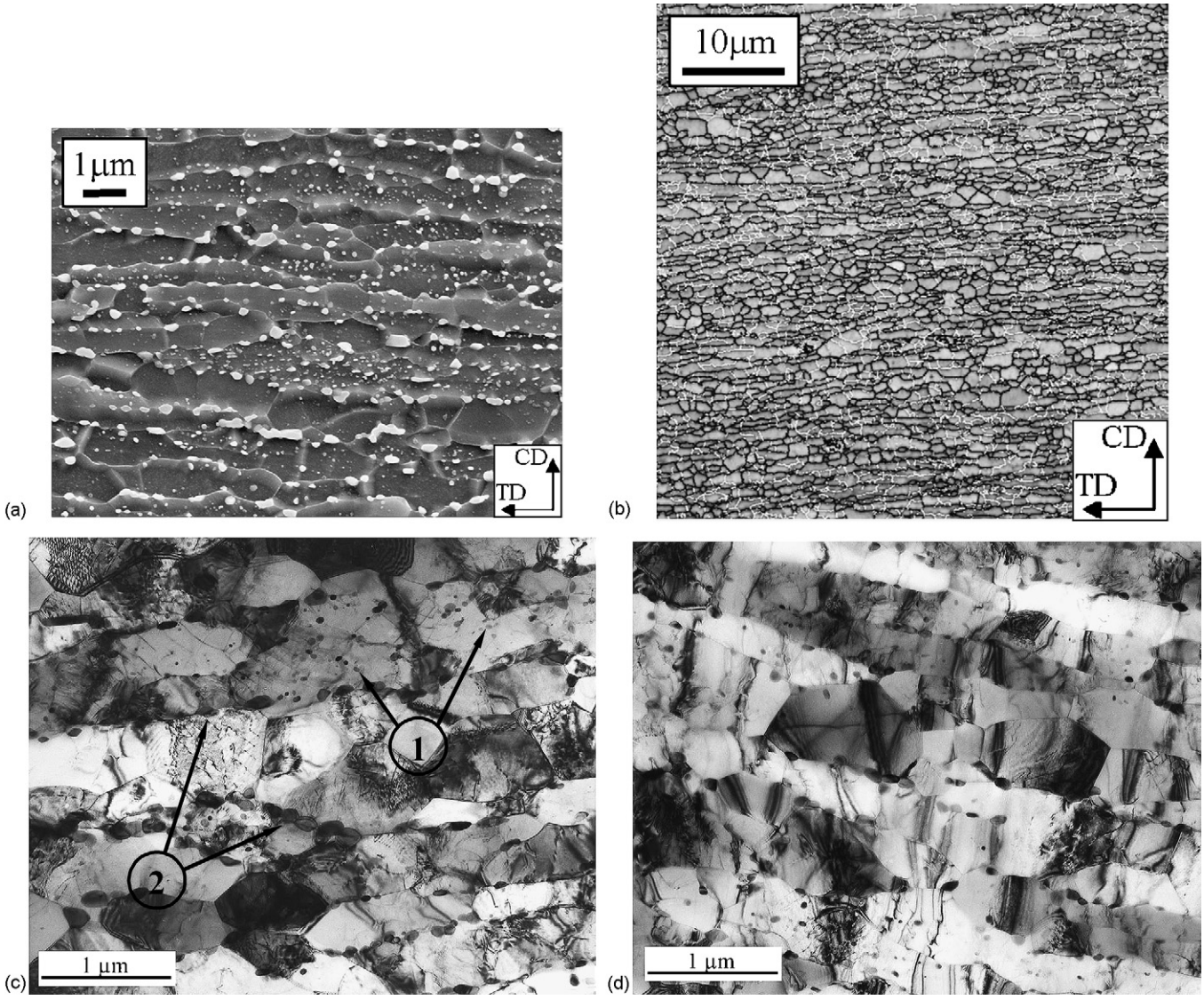

Fig. 1. SEM image (a) and EBSD map (b) after large-strain deformation ($\varepsilon = 1.6$) and subsequent 2 h annealing at 823 K obtained for a plain C–Mn steel (CD, compression direction; TD, transition direction). The black lines indicate grain boundary misorientations between 15° and 63°. White lines indicate grain boundary misorientations between 2° and 15°. (c) TEM micrograph of an ultrafine grained steels after large strain warm deformation ($\varepsilon = 1.6$, and 2 h at 823 K) with 0.74 mass% Mn. Arrows "1" point at very fine cementite particles inside the ferrite grains; arrows "2" point at coarse cementite particles at the ferrite grain boundaries. (d) Corrresponding TEM micrograph for a steel with 1.52 mass% Mn. Details of the compositions and of the processing are given in [39–45].

SPD methods. An important issue in this context, however, is that in the case of large sample sizes the strain and cooling paths have to be carefully controlled since they are key parameters that govern the final grain size within relatively small process windows.

A further difference between these two approaches is that the advanced thermomechanical methods are continuous processes and can be well optimized when they work in a temperature regime where they exploit phase transformation and controlled cooling. The most significant feature of transformation refinement is the possibility of optimizing the conditions to produce a maximum number of new grains that usually nucleate at grain boundaries. In this context, the high temperature phase can be pretreated to increase the grain boundary area (refined or pancaked grains) and to introduce a dense dislocation substructure by large strains at the lowest possible temperature to avoid static primary recrystallization. Ultimately, the transformed product can be subjected to warm or cold deformation, possibly in conjunction with precipitation of carbides in steel. A concern in this context is not only the desired increase in strength but also the possible drop in toughness and ductility [61].

2.4.2. Similarities

Ultrafine grained ferrite microstructures are of great interest for low alloyed structural steels as reflected by the steels reported in Table 1, regardless of severe plastic deformation or advanced thermomechanical processes. Structural steels with improved mechanical properties may facilitate light-weight construction design (buildings, bridges, large structures). Both the SPD and advanced thermomechanical processes may encounter difficulties in being scaled up to large commercial scales and

Table 1
Summary of different techniques reported to produce ultrafine grains in bcc steels

Techniques	Steels	Steels composition (wt.%)	Ferrite grain size achieved (μm)	Log. strain imposed [1]	Deformation temperature (K)	Heat treatment after deformation	Reference
ECAP	Plain low carbon steel	0.08C–0.42Mn–0.18Si	0.2	3.0	293	AC	[7]
	Plain low carbon steel	0.15C–1.1Mn–0.25Si	0.3 in thickness	4.0	623	AC	[22]
	Ti–V carbon steel	0.1C–1.59Mn–0.29Si–0.02Ti–0.05V	∼0.3 in thickness	1.0	573	AC	[59]
	Ferrite–martensite dual phase steel	0.15C–1.06 Mn–0.25Si	0.8	4.0	773	1003 K × 10 min WQ	[46]
ARB	Ti added IF steel	0.003C–0.15Mn–<0.01Si–0.049Ti	0.4	5.6	773	WC	[14]
HPT	Plain low carbon steel	∼0.7C–∼1.0Mn–∼0.3Si	0.01	Shear strain 300, log. strain 0.45	293	AC	[16,18]
DRX* during hot deformation	Microalloyed steel	0.11C–1.45Mn–0.34Si–0.068Nb	2–5	Final rolling 2.2–3.6	1153–1033	AC	[26]
Strain-induced ferrite transformation	Plain low carbon steel	0.06C–0.59Mn	1.0 (strip surface)	0.36	1053	AC	[27]
Deformation in the intercritical region	Plain low carbon steel	0.17C–1.32Mn–0.44Si–0.15Nb	2.1	2.3	973	WQ	[60]
Warm rolling in the ferrite region	Ti added IF steel	0.003C–0.15Mn–0.022Si–0.065Ti	1–3	Final rolling ∼0.55 × 5	Below A^*_{r1}	WQ	[34]
DRX* of ferrite during warm deformation	Ultra-low carbon steel	0.0016C–0.1Si–0.3Mn	–	4.0	723–823 (lower than A^*_{c1})	WQ	[36]
Pronounced recovery of ferrite during warm deformation and annealing	Plain medium carbon steel	0.22C–0.21Si–0.74Mn	1.3	1.6 at strain rate of 0.01 s^{-1}	823	823 K × 120 min	[39]
Cold deformation and annealing of martensitic steel	Martensitic steel	0.13C–0.37Mn–0.01Si	0.18	0.8	293	773 K × 30 min	[49]

Abbreviations: DRX*, dynamic recrystallization; A^*_{r1}, austenite to pearlite transformation temperature during cooling; A^*_{c1}, pearlite to austenite transformation temperature during heating; ECAP, equal channel angular pressing; ARB, accumulative roll bonding; HPT, high pressure torsion; AC, air cooling; WC, water cooling; WQ, water quench.

mass production, but both approaches offer insight into the microstructure and properties that can be achieved by such approaches.

3. Microstructure characterization of ultrafine grained steels

Ultrafine grained ferrite microstructures can be quite different due to the various methods and heat treatments applied as well as the differences in the chemical compositions and the initial microstructures. In this section, characterization of ultrafine grained bcc steel microstructures will be discussed in detail.

3.1. Microstructure of ultrafine grained steels produced by SPD techniques

3.1.1. Equal-channel angular pressing

The microstructures of low carbon steels (0.15 wt.% C) after different passes of equal-channel angular pressing have been investigated by Fukuda et al. and Shin et al. [7,22]. After one ECAP pass ($T = 623$ K, $\varepsilon = 1.0$), the microstructure consisted of extended parallel grain boundaries with mainly low-angle misorientation angle between adjacent crystals [7,22]. The width of the parallel bands was approximately 0.3 μm and the dislocation density inside the subgrains was relatively low. After two ECAP passes ($\varepsilon = 2.0$), the average misorientation between subgrains increased, the ferrite grain shape was less elongated and the average grain size was approximate 0.5 μm. Equiaxed ferrite grains with an average grain size of 0.2–0.3 μm were achieved after four ($\varepsilon = 4.0$) ECAP passes. The fraction of high-angle grain boundaries increased gradually with further deformation passes. Consequently, the final microstructure of samples, which had undergone a sufficient number of ECAP passes consisted mainly of high-angle grain boundaries [7].

For a submicron grained low carbon steel processed by ECAP ($\varepsilon = 4.0$) at 623 K, less grain growth was observed at relatively low annealing temperatures (693–783 K for 1 h) [62]. Both the dislocation structure and the well-defined grain boundaries at elevated temperatures observed in the microstructure demonstrated the occurrence of recovery during annealing in this temperature region. A further increase in the annealing temperature ($\geq$813 K) led to partial primary recrystallization. The addition of Ti and V to low carbon steels did not lead to significant refinement of ferrite after ECAP processing [59]. Nevertheless, very fine Ti–V nitrides were reported to be beneficial for improving work hardening of the steel by accumulation of dislocations around the precipitates.

It is well known that many ultrafine grained single phase steels exhibit relatively low tensile ductility at room temperature. This can be partially attributed to the low work hardening rate, which is commonly observed for ultrafine grained single phase material. One approach to improve the work hardening of such steels is to create microstructures, which contain a second phase. In this context, ultrafine grained dual phase steels seem to be attractive for obtaining both higher strength and improved ductility. Ultrafine grained ferrite–martensite dual phase steels (0.15% C) have been fabricated by Park et al. [48,63] using ECAP plus intercritical annealing in the ferrite/austenite two phase region (i.e. between the A_{c1} and A_{c3} temperatures) followed by quenching. The microstructure of the steel after the ECAP deformation ($T = 773$ K, $\varepsilon = 4.0$) consisted of a severely deformed pearlitic lamellar microstructure with reduced interlamellar spacing, ultrafine ferrite with an average grain size of 0.2–0.5 μm with high dislocation density, and spheroidized cementite particles. After intercritical annealing at 1003 K for 10 min and subsequent water quenching, the microstructure consisted of ultrafine ferrite grains, homogeneously distributed martensite islands, and incomplete martensite networks at the ferrite–ferrite grain boundaries. The martensite islands were transformed from the austenite, which replaced pearlite during the intercritical annealing treatment. The martensite network was reported to be associated with local segregation of Mn [48,63]. High dislocation densities were observed in the ferrite grains adjacent to the martensite. Most of these dislocations were assumed to result from accommodation of the phase transformation during quenching. The high dislocation density enhanced the work hardening behavior. In summary, grain refinement was significant after the first pass of ECAP. A further increase in the number of deformation passes had a diminishing effect on grain refinement but was beneficial for the formation of high-angle grain boundaries and the transition of the ferrite grain morphology from an elongated to more equiaxed shape. The ultrafine grained microstructure produced by ECAP was relatively stable against grain coarsening at certain temperatures. Recovery was the main softening mechanism at modest annealing temperatures.

3.1.2. Accumulative roll bonding

Compared with the ultrafine grained microstructure produced by the other SPD and conventional rolling techniques, different types of microstructures and crystallographic textures were observed for steels produced by the ARB method [23,64,65]. This difference can be attributed to the different strain distributions associated with the various approaches. It is well known that the surface regions of ferritic steel sheets processed by large strain rolling reveal a pronounced shear texture which is quite different than the texture observed in the through-thickness center regions of the same sheet [66–69]. In the ARB technique, the rolled sheet is cut and stacked between ensuing cycles, so that half of the surface, which had undergone the severe shear deformation in the prior rolling step ends up in the sheet center in the following ARB rolling step. These shear regions appear not only at the surface layers, but are also distributed through the sheet thickness after several ARB passes. Materials processed by ARB undergo a complicated mixed series of plane strain and shear deformation states. Thus, steels processed by the ARB method experience a complex distribution of microstructure and texture through their sheet thickness [23,64,65].

Tsuji et al. [23,64] investigated the microstructure and crystallographic texture of an ultra-low carbon (0.003% C) IF steel processed by the ARB process. Experiments were conducted by imposing a logarithmic strain of $\varepsilon = 0.8$ (50% reduction) at 773 K. This procedure was repeated up to seven cycles corresponding to a total strain of 5.6. The microstructure after one

cycle of the ARB process ($\varepsilon = 0.8$) showed a typical dislocation cell structure. The size and orientation of elongated cells varied through the sheet thickness. After two more cycles of the ARB process ($\varepsilon = 2.4$), elongated grains with high-angle misorientation were observed in addition to the dislocation cell structure. With further increases in strain ($\varepsilon \geq 3.2$) the resulting microstructure consisted mainly of elongated ultrafine ferrite grains, and an increased fraction of high-angle grain boundaries. After seven cycles of the ARB process ($\varepsilon = 5.6$) around 80% ultrafine ferrite grains were surrounded by high-angle grain boundaries, while some dislocations remained in the ferrite. The ultrafine grained microstructure was distributed relatively homogenously throughout the sheet thickness.

The ultrafine grained microstructure formed via the ARB process can be interpreted in terms of a process of repeated gradual recovery and grain subdivision. The extent of recovery is sufficient to result in high-angle grain boundaries after extensive ARB. The ARB method is more effective for achieving grain refinement than conventional routes at identical strains. The authors attributed this to the redundant shear strain throughout the thickness of specimens processed by the ARB, which facilitated grain subdivision and formation of an ultrafine grained microstructure [23,64,65].

3.1.3. High pressure torsion

The thickness reduction imposed on samples processed by HPT is negligible compared to the large shear strain imposed. The formation of nanostructures and the dissolution of pearlite lamella in a commercial pearlitic steel (~0.7% C) produced by HPT were reported by Ivanisenko et al. [16–18]. After a shear strain of 100 at room temperature the microstructure at the surface of a disk shaped sample consisted of a cell structure and partially dissolved cementite lamellae. Further increase in the shear strain to a level of 200 resulted in an inhomogeneous grain morphology. Elongated grains 100 nm in length and 15 nm in height were created during the process. The elongated grains were separated by dense dislocation walls. This morphology was very similar to the lamellar-type boundaries observed in samples processed by ECAP. The spacing of the cementite lamella decreased during straining. After a shear strain of 300, a homogeneous nanostructure with a grain size of 10 nm and total dissolution of cementite was obtained.

3.2. Microstructure of ultrafine grained steels produced by advanced thermomechanical processing

3.2.1. Transformation grain refinement

In low carbon microalloyed steels, ferrite grain sizes and precipitation states are important factors, which affect the strength–toughness relationship. The ferrite grain size is a function of the austenite grain size after austenite recrystallization, the amount of retained strain in the austenite before the start of transformation, and the cooling rate through the transformation regime [56].

Progressive refinement of the austenite can be achieved through dynamic and static recrystallization during large strain deformation (roughing) at temperatures above the recrystallization temperature. According to the work of Kaspar et al. [26], by strictly controlled hot deformation schedules, dynamic recrystallization of austenite is obtained at relatively low temperatures (less than 1143 K) by applying total finishing strains greater than 2.2 in a microalloyed steel (0.11C–0.34Si–1.45Mn–0.068Nb–0.08V, wt.%). The grain size of the dynamically recrystallized austenite was around 1–4 μm. Priestner and Ibraheem [56] reported that fine austenite with grain size of <5 μm could be obtained by reheating a cold-rolled tempered martensite (with finely dispersed cementite) in a Nb microalloyed steel (0.1C–0.31Si–1.42Mn–0.035Nb, wt.%) [56]. Average ferrite grain sizes of <1 μm in the surface layer of a 2–3 mm thick sheet have been achieved using accelerated cooling (e.g. ~8 K s^{-1}) after hot rolling of fine austenite to equivalent strains of 0.5–1.0 at 1123 K [56]. The ferrite grain size in the center of the plate was ~1.5 μm. Studies using EBSD and misorientation imaging showed that most of the grain boundaries revealed misorientations above 15° [56].

Contrary to the accepted view that fine austenite grain sizes lead to fine ferrite grains, Hurley and Hodgson [54] showed that a very fine ferrite grain size could be produced from a steel having a large prior austenite grain size. Intragranular nucleation of ferrite may be an important factor contributing to the additional grain refinement observed when a dynamic strain-induced transformation occurs, and is encouraged by large austenite grain sizes and accelerated cooling, both of which suppress the formation of grain boundary proeutectoid ferrite [54]. The strain-induced transformation rolling procedure is attractive in terms of its relative simplicity and ability to refine ferrite grain sizes in plain carbon steels [70–75]. The technique involves rolling steel strip containing a large austenite grain size (>100 μm), at a temperature just above the A_{r3} but below the A_{e3}. A single rolling pass induces very efficient grain refinement, producing equiaxed and fine polygonal ferrite grains on the scale of less than 2 μm in the surface regions (~250 μm deep) of the strip [53]. The rolling reduction required to generate this ultrafine ferrite is approximately 35–40%. It appears that a roll chilling effect in conjunction with large shear strains resulting from roll friction explain the phenomenon. These steps facilitate a high density of intergranularly nucleated ferrite grains during hot rolling of austenite.

Using large strain ($\varepsilon = 2.3$) hot rolling in the austenite/ferrite two-phase region, followed by fast cooling, Nanba et al. [60] produced ultrafine ferrite with a grain size of 1.2 μm in a low alloyed steel (0.17C–0.44Si–1.32Mn–0.015Nb, wt.%). In contrast, Bodin et al. [76] reported that a bimodal grain size distribution was obtained by hot rolling in the two-phase region. Conceivably, the large ferrite grains (>6 μm in diameter) observed in the bimodal size distribution can be attributed to growth of the transformed ferrite into the deformed ferrite. The transformed ferrite resulted from austenite that was deformed during intercritical rolling, while the deformed ferrite was transformed from austenite before intercritical rolling. The small ferrite grains (1–2 μm in diameter) were attributed to extended recovery of the deformed ferrite [76]. In order to obtain homogeneous ultrafine ferrite by intercritical rolling, it seems to be very important to balance the dynamic transformation of austenite into ferrite and the dynamic

recovery and recrystallization of ferrite through careful control of the processing parameters including chemical composition, deformation schedules (strain/strain rate/temperature), and cooling rate. For example, low carbon steels have a relatively small intercritical regime and recrystallization of deformed ferrite can proceed rapidly but is terminated upon rapid cooling.

3.2.2. Grain refinement by recovery/recrystallization in warm working

Since hot working involves a high cost of thermal energy, there has been a trend to develop processes at lower temperatures [77]. Deformation at lower temperature, also referred to as warm working, can help to produce steels close to their final shape and reduce or eliminate cold work involving higher roll forces or die-pressures. Grain refinement during warm or ferritic rolling can be realized by recovery/recrystallization. In this context, dynamic recrystallization of ferrite under conditions of temperature and strain rate that correspond to a large Zener–Hollomon parameter, i.e. at low temperatures and high strain rates, is more beneficial to obtain good microstructure homogeneity.

In contrast to the accepted view that grain refinement is achieved by recrystallization, Song et al. [40,44] have recently proposed that pronounced or extended recovery is more effective for the formation of ultrafine microstructure. In their studies, the prevalence of primary recrystallization instead of recovery was not generally beneficial since it significantly reduced the dislocation density and removed the substructure that was important for the gradual formation of subgrains and of ultrafine grains surrounded by HAGBs.

3.2.3. Grain refinement by cold deformation and annealing

It is known that the grain size obtained by static recrystallization is a function of the prior strain and the prior grain size [56]. Cold rolling and annealing of an initial martensite microstructure have drawn some attention recently to produce multiphase ultrafine grained steels [49–51]. The initial fine martensite is beneficial for grain subdivision during cold rolling due to the high dislocation density and substantial amount of solute carbon atoms in martensite. Nearly equiaxed ferrite grains and a homogeneous distribution of carbides were found after annealing. A multiphase ultrafine grained steel, consisting of ultrafine ferrite, dispersed cementite and tempered martensite, showed a good combination of strength and ductility.

3.3. Summary: production of ultrafine grained microstructures

In order to more quantitatively evaluate the microstructure of ultrafine grained steels, it has become customary to report not only the average cell or grain sizes and the corresponding grain size distributions, but also the fraction of high-angle grain boundaries obtained from the various processing strategies. The submicron structure produced by SPD is typically more elongated due to the intense deformation involved. Around 40% of the grain boundaries are of the low-angle dislocation boundary type (misorientations $< 15^\circ$), which is less beneficial for the overall mechanical response. These low-angle grain boundaries often appear in TEM as dense dislocation walls, rather than as sharp boundaries, which could migrate more easily. It is difficult for the cells to be transformed into discrete grains surrounded by high-angle grain boundaries without an annealing treatment. The conversion to high-angle misorientation walls usually occurs at a temperature of 0.3–0.4T_M (melting temperature), which is much below the traditional static recrystallization temperature of 0.5T_M [61].

Hot deformation develops larger more polygonized cells or subgrains during dynamic recovery compared to the submicron structure produced by SPD. Increasing strain leads to the occurrence of dynamic recrystallization of austenite. Hot working at intermediate temperature often provides a mixed microstructure of different grain sizes. Warm and cold working hastens grain subdivision due to a relatively higher dislocation density introduced/accumulated compared to hot deformation. Subsequent annealing is beneficial for formation of high-angle grain boundaries by pronounced recovery/recrystallization processes.

The effects of alloying are largely similar in the different types of processing. Solid solution additions usually increase the degree of strain hardening in both cold and hot working and may slow dynamic recovery in bcc steels. Large quantities of second phase constituents, such as fine cementite particles, are beneficial for the formation of a fine ferritic grain structure. They inhibit grain boundary migration due to Zener pinning. This effect stabilizes the ultrafine grains against grain coarsening, and is also thought to inhibit primary recrystallization. The presence of such fine particles results in an increase of the effective recrystallization temperature, widening the temperature windows for corresponding warm rolling and annealing treatments [39].

4. Tensile properties

4.1. Strength

4.1.1. Effect of grain size on strength

The yield stress for bcc steels processed by different methods is plotted in Fig. 2 as a function of the inverse square root of the grain size for grain sizes ranging from 45 to 0.2 μm. The ultrafine microstructures (grain size less than 2 μm) were produced by various techniques: the open symbols display the results from the SPD methods; the full symbols in gray represent the results from the advanced thermomechanical process routes (ATP); the full symbols in black show the results from the conventional route (Conv). For each class of steel, the yield stress follows the Hall–Petch relation for a given steel, $\sigma_y = \sigma_i + k_y d^{-1/2}$, where σ_y is the yield stress, σ_i the friction stress, k_y the grain boundary resistance and d is the grain size in μm.

The lower yield strength of the 0.13C–0.67Mn–0.14Si (wt.%) steel sheet produced by cold rolling and annealing [82] is shown by the solid diamond in Fig. 2 where the grain size varied from 1.6 to 30 μm. The friction stress σ_i is about 100 MPa and the grain boundary resistance k_y is 551 MPa $\mu m^{1/2}$ [82], according to the work of Morrison in 1966.

ECAP (at 623 K) followed by annealing at temperatures between 373 and 873 K produced steels with grain sizes rang-

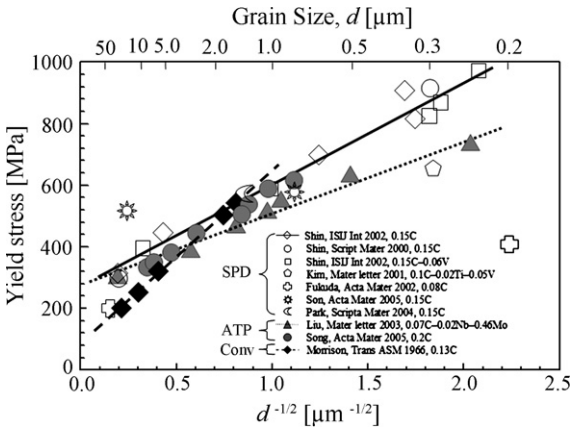

Fig. 2. Hall–Petch relationship in ultrafine grained bcc steels [7,46,48,59,78–82]. The open symbols display the results from the SPD methods; the full symbols in gray represent the results from the advanced thermomechanical process routes (ATP); the full symbols in black show the results from the conventional route (Conv). The straight lines show the Hall–Petch relation for different steels.

ing from about 0.23 to 10 μm in a low carbon (0.15C–1.1Mn –0.25Si, wt.%) and a low alloy steel (0.15C–1.1Mn–0.25Si–0.06V, wt.%) [78]. The k_y value in Fig. 2 (slope of bold line) is smaller in the steel processed by ECAP compared with the results of Morrison (dashed bold line). The yield stress for a grain size of 30 μm before ECAP is above the value predicted by Morrison, while the yield stress after ECAP is below the line. This phenomenon also reappears in other studies from both SPD and advanced thermomechanical processes [7,46,48,59,79–81]. That is, while the Hall–Petch relationship in steels may extend to the submicron range, the parameter k_y may decrease. The reason for this behavior will be discussed in Section 4.1.3.

For steels with submicron grain sizes produced by ECAP, the yield stress for steels with a carbon content less than 0.1 wt.% [7,59] is notably smaller than for the steels with 0.15 wt.% carbon [78] for a given grain size. The reason for this behavior is not fully understood, but could result from differences in grain size measurement.

The data for samples with a dual phase microstructure (displayed by the sun symbol in Fig. 2) [46] do not follow the line predicted by the Hall–Petch relationship as mentioned above. It seems that a smaller increment in stress is achieved in the dual phase steel when the ferrite grain size is refined from 19.4 to 0.8 μm. It is not clear whether this is related to some variation in the amount and morphology of the second phase after grain refinement.

4.1.2. Summary of Hall–Petch analysis for bcc steels

It should be stressed that in early investigations by Morrison [82], as shown in Fig. 2, the different grain sizes were produced by cold rolling and subsequent annealing at different temperatures. This offered the advantage to alter only one parameter—the grain size. In the investigation by Song et al. (where the initial motivation was not to measure the value of k_y and σ_i in the Hall–Petch equation), the coarse microstructure consisted of conventional ferrite and pearlite. When refined into the ultrafine microstructure, however, it comprised ferrite and fine spheroidized cementite. A smaller k_y value was found by Shin et al. [79], which might also be attributed to the change in overall microstructure (along with grain size) in their study. By use of the ECAP technique, the initial coarse grained ferrite–pearlite microstructure was severely deformed. After four deformation passes, a microstructure with finer ferrite and a partially spheroidized pearlite was obtained. Thus, the smaller k_y value in some studies on ultrafine ferrite might be the result of a reduction in the yield strength by replacing harder pearlite with softer ferrite and spheroidized cementite in the ultrafine microstructure. The presence of low misorientations between some grains in the ultrafine ferrite may also contribute to the reduced k_y value in comparison to conventional "coarse" ferrite with high misorientations.

It should be mentioned that most of the submicron microstructures measured for the SPD technique consist of large quantities of low-angle grain boundaries, and grain dimensions measured refer to the thickness of stretched microbands, which is not the same as average grain diameter. Further consideration of grain morphologies and appropriate characterization methods may be worthwhile to define the Hall–Petch relationship more accurately.

4.1.3. Comments on the effect of ultra grain refinement on the Hall–Petch k_y value

A series of early experimental investigations using Armco iron and nickel [83,84] over a broad range of grain size showed that the Hall–Petch relationship was an approximation applicable only over a limited range of grain sizes. The value of k_y seems to decrease for very small grain sizes. This deviation of the Hall–Petch relationship has been noted since the late 1950s and early 1960s [85–88]. Efforts have been made to develop an understanding of this behavior.

For polycrystalline materials, there exist three main theories for the Hall–Petch equation: the pile-up models [86,89–91], those based on work hardening [88,92,93] and the grain boundary source theories [94,95]. Pande et al. [96] demonstrated that the decrease of k_y at small grain sizes can be explained within the framework of the traditional dislocation pile-up model. The solution of the pile-up problem for small numbers of dislocations ($n < 20$) differs considerably from the usual solution [97] valid for larger n. With smaller grain sizes the $\sigma_y(d^{-1/2})$ relationship becomes a staircase function that reaches a plateau equal to $\sigma_y^{max} = M\tau_c$ at $n = 1$, where M is the Taylor factor and τ_c is the critical shear stress required for dislocation motion.

Fig. 3 shows a comparison of calculated exact and approximate n values together with the Hall–Petch prediction. It can be observed from Fig. 3 that the linear Hall–Petch relation is valid for this model when $n > 20$. If the length of one pile-up is assumed to be equal to half of the grain diameter, L, when n is equal to 20, the grain size/diameter is about 0.79 μm. This means based on the prediction in Fig. 3 a smaller k_y value results when the grain size is less than 0.79 μm. According to the results from SPD as displayed in Fig. 2, k_y maintains the same value when grain size is varies from 10 to 0.23 μm for a given steel. Therefore, it can be concluded that the smaller value of k_y in the present study is not fully explained by the model discussed above.

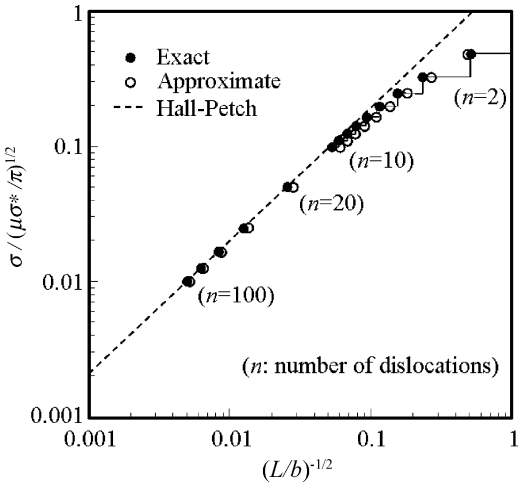

Fig. 3. Comparison of the exact and approximate n value (number of dislocations) together with the Hall–Petch prediction. After [96]. The exact value is calculated from the data of [98]. The approximate curves exhibit discrete steps and begin to level off as described by [99]. L is the length of the pile-up which is associated with the grain size, b the magnitude of Burger's vector, σ the applied stress and σ^* is the barrier stress which is assumed to be constant and independent of grain size; μ is the shear modulus.

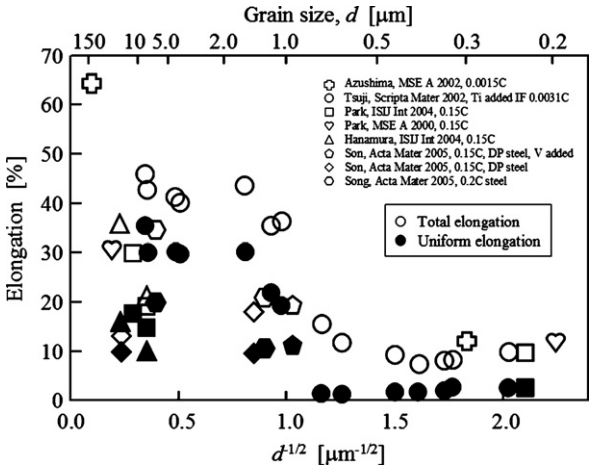

Fig. 4. Grain size dependence of ductility for bcc steels [24,44,46,102–105]. Open symbols represent total elongation while filled symbols display uniform elongation in tension.

Recent studies have reduced grain sizes to a few nanometers. Compared to conventional polycrystalline materials, nanocrystalline materials have often been found to exhibit a smaller or even a negative Hall–Petch slope. The critical grain size where deviation from Hall–Petch relation occurs is dependent on the specific material of interest [100].

4.2. Ductility

Several groups [27,40,52,101,102] have reported promising room temperature tensile strength properties for ultrafine grained steels. The steels are produced either by the severe plastic deformation or by the advanced thermomechanical processes. Many of the ultrafine grained steels investigated do not display a significant amount of work hardening, however. This shortcoming is reflected in high yield ratios (lower yield stress to ultimate tensile stress). For many ultrafine grained steels, the yield ratios are almost 1.0, compared to 0.7 for conventional steels with similar alloy content.

Reduced work hardening typically leads to low tensile ductility in ultrafine grained steels. According to the work of Park et al. [102], an ultrafine grained low carbon steel (0.15C–1.1Mn–0.25Si, wt.%) with a grain size of 0.2 μm, manufactured by severe plastic deformation (accumulative equivalent strain of 4.0 at 623 K), exhibited no work hardening, i.e. necking occurred already in the Lüders regime. Therefore, only a small "uniform" elongation was reported. As an example, Fig. 4 provides data on tensile ductility versus inverse square root of grain size for bcc steels with grain sizes of 150–0.2 μm. For each of the steels, the total elongation is represented by an open symbol and the uniform elongation is displayed by a filled symbol. The figure shows that a decrease in grain size leads to a decrease in ductility. A sudden drop of elongation at a grain size of about 1 μm was reported in the study by Tsuji et al. (circles) for an IF steel refined by the ARB process at 773 K and subsequent annealing [24]. It is interesting to note that this tendency does not apply to the ultrafine grained dual phase steel (diamonds) according to Son et al. [46], produced by ECAP with an effective strain of around 4.0 at 773 K and subsequent intercritical annealing at 1003 K for 10 min. The uniform elongation was higher for the ultrafine grained dual phase steel (the sizes of the ferrite grains and martensite islands were about 0.8 μm), while the total elongation was comparable to its coarse grained counterpart, having ferrite grain and martensite island diameters of about 19.4 and 9.8 μm, respectively. The authors attributed the better ductility in the ultrafine grained dual phase steel to extensive work hardening associated with a high density of mobile dislocations.

The decrease in tensile ductility at room temperature for most of the ultrafine grained steels, especially single phase steels, can be explained as follows. First, dynamic recovery as a softening mechanism is able to reduce the apparent work hardening rate. During deformation, dislocations that carry the intragranular strain are trapped at grain boundaries. The kinetics of dynamic recovery are associated with the spreading of trapped lattice dislocations into grain boundaries especially in ultrafine grained steels [106–108]. The change of the dislocation density during dynamic recovery in terms of the trapped lattice dislocations spreading into the grain boundaries was studied in detail by Park et al. [102]. The authors calculated approximate recovery times for dislocations moving into grain boundaries, and showed that for ultrafine grained steels the time for dislocations moving into grain boundaries is shorter than the time of the tensile test. This decrease in dislocation density reduces accumulation of dislocations inside grains, and consequently leads to less work hardening when compared with corresponding steels of large grain size. Following these earlier investigations, it is suggested that there are two kinds of recovery mechanisms, namely, slow recovery in the grain interiors and much faster recovery in the vicinity of grain boundaries. In coarse grained steels, the latter mechanism is less important due to the lower volume fraction of material near grain boundaries. Taking the study of Song et

al. [44] for example, a plain carbon steel (0.2 wt.% C) grain diameter was reduced from 6.8 to 1.3 μm. This grain refinement enhanced the fraction of the overall volume near grain boundaries by a factor of about 143. Thus, in ultrafine grained steels, faster recovery near grain boundaries seems to be important.

Second, the decrease in tensile ductility can be explained in terms of plastic instability, which initiates necking due to localized deformation. The condition for initiation of necking in a uniaxial tensile test is indicated by the Considère criterion [109], $\sigma_t = d\sigma_t/d\varepsilon_t$. When the slope of the true-stress true-strain curve (work hardening rate), $d\sigma_t/d\varepsilon_t$, is equal to the true stress, σ_t, uniform deformation stops and necking is initiated. As mentioned above, ultra grain-refinement greatly increases the flow stress of steels, especially during the early stages of plastic deformation. Grain refinement also leads to reduced work hardening capacity. As a result, plastic instability (necking) occurs at an early stage during tensile testing, which results in limited uniform elongation in ultrafine grained steels.

The yield ratio is high in ultrafine grained steels. However, according to the study by Song et al. [44], good ductility can still be obtained in 0.2% C steel, as documented by a total elongation of about 20% and uniform elongation of about 10% (Fig. 5). These values differ from the results reported in previous studies, where total elongations are usually below 10%. The high ductility observed by Song et al. was attributed to the presence of finely dispersed cementite particles, which increase the work hardening rate [42]. A large volume fraction and a fine dispersion of cementite effectively increase the work hardening rate by promoting accumulation of dislocations around the particles [110,111]. Another approach to improve the tensile ductility of ultrafine grained steel at room temperature is to adopt a composite structure in which only the surface is ultrafine, while the core with a coarse microstructure provides ductility. An interesting extension of this idea is to employ ultrafine grains locally, only where they are needed in the product to locally generate high strength and toughness [112].

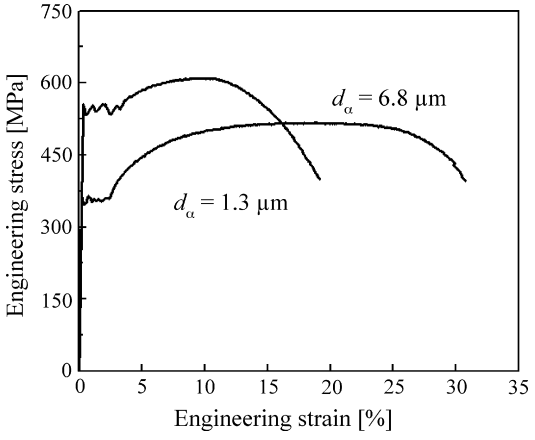

Fig. 5. Comparison of engineering stress–strain curves of the 0.2% C steels with different ferrite grain sizes. The different grain sizes were produced by the conventional route (without large strain warm deformation) and the ultrafine grain route, respectively. The ultrafine grain route involved a warm deformation procedure with four steps (each deformation step with $\varepsilon = 0.4$ and $\dot{\varepsilon} = 10\,s^{-1}$) and a subsequent 2 h annealing treatment at 823 K. The symbol d_α refers to the average ferrite grain diameter. After Song et al. [44].

4.3. Lüders strain

It is well known that a decrease in grain size leads to an increase in Lüders strain as illustrated in Fig. 5 [44]. A large Lüders strain has also been noted by Lloyd and Morris [113] in a fine grained (1–3 μm) Al–6% Ni alloy that contained small amounts of magnesium in solid solution. They observed that the reduction of grain size entailed an increase in yield stress and a decrease in work hardening. Hayes and Wang [114,115] conducted a study on the influence of grain refinement on Lüders strain in Al alloys. They investigated the serrated strain regime for specimens with various grain sizes between 0.4 and 20 μm and observed that the Lüders strain was linearly proportional to the inverse square root of the grain size in Al alloys, as in the Hall–Petch relationship. The appearance of pronounced yield drops and very large Lüders strain regimes thus appear to be characteristics of ultrafine grained Al alloys as well as steels [44,114]. These phenomena can be linked to an instantaneous low density of mobile dislocations, lack of dislocation sources within grains, and the low work hardening rate of ultrafine grained alloys.

The serrated flow that characterizes the propagation of plastic strain within a Lüders band is governed by the dynamic interplay of micromechanical hardening and softening. The Lüders regime is determined by the population of mobile dislocations, the strain hardening coefficient, the strain softening coefficient, the strain rate and temperature [42]. Song et al. [42] reported that yielding involved the initiation of deformation bands due to local stress concentrations. Owing to the high density of mobile dislocations formed by unlocking and by dislocation multiplication, the material within the deformation band effectively softens and undergoes localized plastic deformation. As mentioned in Section 4.2, dynamic recovery is pronounced in steels with smaller grain sizes owing to fast recovery in the vicinity of grain boundaries [102]. A decrease in the work hardening rate in the ultrafine grained steel, which can be attributed to the rapid dynamic recovery, favors a non-uniform deformation mode like local deformation by Lüders bands. This leads to slow propagation of the Lüders band front in the steel with a fine microstructure. The slow propagation is coupled with a large Lüders strain.

5. Toughness of ultrafine grained bcc steels

5.1. Toughness improvement in ultrafine grained steels

While several studies examined tensile properties of ultrafine grained steels, Charpy impact properties were less commonly investigated due to limitations in the sample size typically available from laboratory-scale process set-ups.

The impact properties of ultrafine grained IF, low/medium carbon and Nb–V–Ti microalloyed steels have been reported by Tsuji et al. [116], Hanamura et al. [105], Song et al. [44] and Sjong et al. [117]. Fig. 6 shows the impact transition curves of the medium carbon steels (0.2 wt.% C) for subsize (3 mm × 4 mm) specimens [44]. Compared with conventional steel (grain size: 6.8 μm), the upper shelf energy is lower and the transition

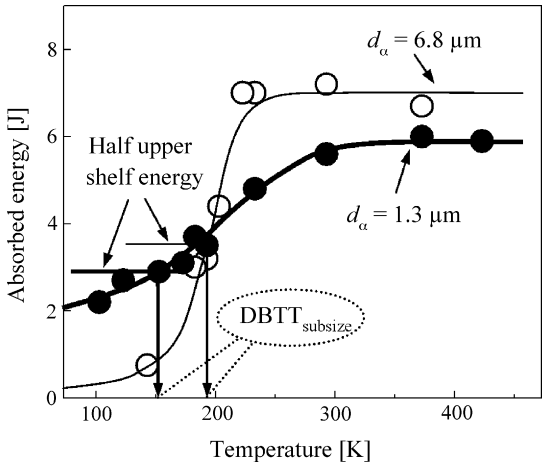

Fig. 6. Dependence of the Charpy impact properties on temperature of the steels with different ferrite grain sizes [44]. The symbol d_α refers to average ferrite grain diameter. DBTT$_{subsize}$: ductile-to-brittle transition temperature of subsize specimen with a 1 mm notch depth and a ligament size of 3 mm × 3 mm. The ductile-to-brittle transition temperature was determined by using the correlation procedure recommended in [118].

region occurs over a wider temperature range in the ultrafine grained steel (grain size: 1.3 μm). The ductile-to-brittle transition temperature was defined as the temperature at half of the upper shelf energy [44]. Fig. 6 shows the decrease in ductile-to-brittle transition temperature (from 193 to 153 K) associated with grain refinement into the ultrafine ferrite regime. In the ductile-to-brittle transition region, the temperature dependence of the absorbed energy is reduced for the ultrafine grained steel. Currently, there is insufficient data to report quantitatively on the relationship between grain size and toughness in the ultrafine and nanocrystalline regime.

5.2. Fundamental explanation for the low ductile-to-brittle transition temperature in ultrafine grained steels

5.2.1. Effect of grain refinement on improving toughness

A reduction in the average grain size commonly leads to a lower ductile-to-brittle transition temperature. This can be understood in terms of cleavage crack initiation and propagation. It is known that the grain size is one of the major factors determining the cleavage fracture unit [119,120]. A decrease in grain size can limit the propagation of initiated cleavage cracks and raise the fracture toughness in the transition region. Since the ductile-to-brittle transition temperature is the point at which the yield stress is equal to the cleavage fracture stress, the ductile-to-brittle transition temperature is lowered by grain refinement due to a more significant increase in the cleavage fracture stress than in the yield stress.

5.2.2. Effect of delamination on lowing the ductile-to-brittle transition temperature

Delamination behavior in Charpy specimens has been reported by several researchers [44,116,121–124]. As shown in Fig. 7, a decrease in grain size or Charpy impact testing temperature leads to an increase in the number of delaminations.

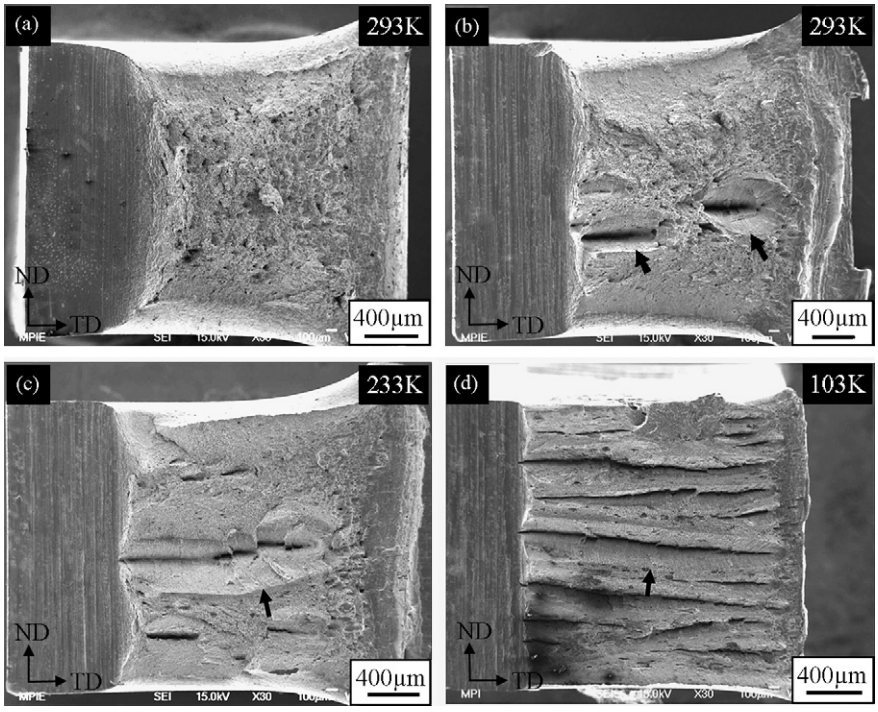

Fig. 7. Scanning electron microscope (SEM) images of fracture surfaces for the steels with different ferrite grain sizes after subsize (3 mm × 4 mm) Charpy V-notch impact tests. (a) Fracture surface of the conventional 0.2% C steel (average ferrite grain diameter of 6.8 μm) after impact testing at 293 K; (b–d) fracture surfaces of the ultrafine grained 0.2% C steel (average ferrite grain diameter of 1.3 μm) after impact testing at 293, 233 and 103 K, respectively. The black arrows point out material delaminations. After [44].

The origin of the delaminations is not completely understood at present. From previous studies it seems that distorted ferrite–pearlite microstructures [125], elongated ferrite grain shapes [121], certain texture characteristics [44,124,126], and aligned particles and inclusions [44,127] favor the occurrence of delamination. However, the phenomenon of delamination does not have a direct influence on the speed of crack growth in ductile failure [128]. Nevertheless, delamination leads to a reduction of the ductile-to-brittle transition temperature in the impact test samples of the ultrafine grained steel due to a decrease in the triaxiality of the stress state [44].

5.3. Shelf energy

The ductile-to-brittle transition in steels is associated with two different failure mechanisms. At high temperatures in the upper shelf region, fracture occurs by nucleation and coalescence of microvoids entailing ductile tearing. This process requires extensive plastic deformation and large amounts of energy. At low temperatures, fracture occurs by cleavage, which is the sudden separation of atomic planes across the specimen [125,129]. In this case, less energy is required.

5.3.1. Lower shelf energy

Fig. 6 shows that the lower shelf energy is significantly higher in the ultrafine grained steel than in the coarse grained steel. On the one hand, this can be attributed to the effect of grain refinement on improving toughness even at very low temperatures. This behavior is shown by the presence of about 50% shear fracture in the ultrafine grained subsize specimen when the test temperature was as low as 103 K. Low temperature toughness can also be enhanced by anisotropic microstructure or pronounced crystallographic texture of the ultrafine grained steel produced by the large strain deformation below the A_1 temperature (austenite to pearlite transformation finish temperature) [44].

Fig. 8a shows the fracture surface of an ultrafine grained 0.2% C steel after Charpy impact testing at 103 K. The high-magnification view of the fracture surface in Fig. 8b clearly shows the smooth delamination surface as well as the dimpled ductile fracture area. The smooth undulating surface suggests some type of decohesion of the grain boundaries. Fig. 8c shows delaminations in the rolling direction, and Fig. 8d shows delaminations following the elongated grain boundaries. The occurrence of delamination along the grain boundaries, both above and below an elongated grain, indicates that the crack can make minor adjustments in its propagation direction switching from one grain boundary to another. This is also confirmed by the observation that two elongated grains (i.e. grain "1" and grain "2" in Fig. 8d) with different texture components, ⟨1 1 1⟩ ∥ ND and ⟨0 0 1⟩ ∥ ND, respectively, were separated by a crack. The delaminations appear to propagate by means of a low-energy fracture mechanism that produces a fairly smooth fracture surface. This fracture does not exhibit the typical cleavage appear-

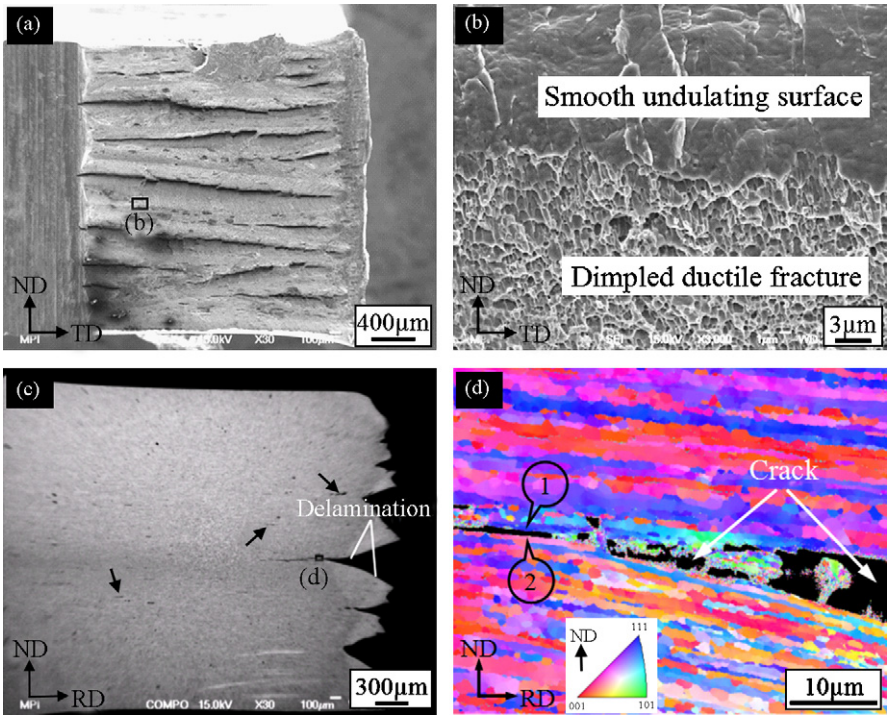

Fig. 8. SEM micrographs and ND (normal direction) orientation map (taken by electron backscatter diffraction (EBSD) measurement) of ultrafine grained 0.2% C steel (average ferrite grain diameter of 1.3 μm) after subsize Charpy impact testing at 103 K. The images shown in (a) and (b) are taken from a plane normal to the rolling direction (RD), while (c) and (d) are normal to the transverse direction (TD) of the sample. Orientation components in (d), ⟨1 1 1⟩ ∥ ND in blue, ⟨0 0 1⟩ ∥ ND in red and ⟨1 0 1⟩ ∥ ND in green. After [44]. (a) Overall fracture surface; (b) transition between delaminated and shear fracture regions. The observation area of (b) is shown in (a). (c) Longitudinal cross-section. The black arrows point out chains of large voids in the specimen; (d) crack propagation along interfaces. The circles 1 and 2 show two elongated grains with high-angle grain boundaries in between. The observation area of (d) is shown in (c).

ance with a strong (1 0 0) texture [121] and contributes to a higher fracture toughness in the lower shelf energy region for the ultrafine grained steel investigated due to reduced triaxiality of the stress state [44]. According to Song et al. [44], a high-angle grain boundary can act as a favorable path for crack propagation especially when large cementite particles are located along the boundary. An alternating microstructure of ferrite and aligned cementite can facilitate the spread of cracks in both the transverse and rolling directions.

5.3.2. Upper shelf energy

A reduced upper shelf energy can be observed in Fig. 6 in the ultrafine grained steel compared with a conventional steel of the same composition. This may be due to the relatively low work hardening and ductility of this steel, consistent with the smaller integrated area below the engineering stress–strain curve, Fig. 5. Delaminations in the ultrafine grained steel observed in the upper shelf region may also contribute to the reduced upper shelf energy.

Compared to the shear fracture surface in the conventional steel (Fig. 7a), a few delaminations can be observed in the ultrafine grained steel (Fig. 7b) Charpy impact specimen tested at room temperature (in the upper shelf region). Since there is little plastic deformation in the area of the delamination, lower absorbed energy and reduced fracture toughness is not surprising in the ultrafine grained steel (Fig. 7b) compared with the conventional steel exhibiting complete shear fracture (Fig. 7a). This differs from the lower shelf energy region, where a decrease in the ductile-to-brittle transition temperature is evident in the ultrafine grained steel due to the change in the stress triaxiality associated with relaxing σ_{zz}. As a result, reduced upper shelf energy and reduced ductile-to-brittle transition temperature appear characteristic of ultrafine grained steel processed by large strain warm deformation (Fig. 6).

According to the work of Fujioka et al. [130], a reduction of the upper shelf energy was also observed in a 0.16C–0.44Si–1.33Mn–0.012Ti–0.013Nb steel with a grain size of 1.5 μm. The ultrafine grained steel in their study was produced by flat rolling with a total logarithmic strain of $\varepsilon \approx 2.5$ at 973 K. They attributed the reduced value of the upper shelf energy to the elongated grain morphology in the ultrafine grained steel. However, in the study of Nagai [131] the same value of upper shelf energy was found for an ultrafine and a coarse grained steel (0.15C–0.3Si–1.5Mn) with grain sizes of 0.9 and 20 μm, respectively. The ultrafine grained steel was fabricated by warm rolling. The sample was rotated 90° about the rolling direction after each pass in order to conduct multi-directional deformation. The upper shelf energy was unexpectedly high, and was explained by the low impurity level of the steel investigated [131].

According to reports in the literature on the shelf energy of ultrafine grained steels [44,130,131], a reduced value of the upper shelf energy in two-phase ultrafine grained materials may be mainly due to the anisotropic microstructure resulting from the large strain deformation. Currently, large strain deformation at a low deformation temperature is a favorable method to produce ultrafine grained microstructures. Therefore, it might be particularly attractive in the future to develop ultrafine grained steels by the use of relatively lower strains and higher temperatures to develop microstructures with fewer delaminations.

6. Conclusions

Processing, microstructure and mechanical properties of ultrafine grained bcc steels were discussed and compared with several of their coarse grained counterparts. The following conclusions can be drawn based on the interpretations presented in this paper:

(1) Ultrafine grained bcc steels can be produced by severe plastic deformation techniques or advanced thermomechanical processing routes. For the severe plastic deformation methods, a well-designed strain path is more important and also more feasible than a precisely controlled temperature path. The small scale, complexity and the discontinuous nature of these processes suggest that they would require considerable ingenuity and investment to be applied on a high-volume industrial scale. Compared with severe plastic deformation methods, the advanced thermomechanical processing routes are less effective with respect to grain refinement, but they are more efficient with respect to large sample sizes. A further difference between these two approaches is that the advanced thermomechanical methods are continuous processes, require less total strain, and can be readily optimized when they work in a temperature regime where they exploit phase transformation.

(2) The submicron structure produced by SPD is typically more elongated due to the intense deformation involved. Around 40% of the grain boundaries are usually subgrain boundaries (grain boundary misorientations <15°) so that many cells are not actually grains but subgrains which are less beneficial for the overall mechanical response of such specimens. It is difficult for the cells to be transformed into real grains, which are surrounded by high-angle grain boundaries without an annealing treatment.

Hot deformation develops larger more polygonized cells or subgrains as a result of dynamic recovery. Hot working at intermediate temperature often provides a mixed microstructure. Deformation induced grain subdivision is essential for the formation of ultrafine grained microstructures by warm and cold working. Pronounced recovery/recrystallization processes are necessary to form high-angle grain boundaries.

(3) An improved combination of strength and toughness is obtained in ultrafine grained steels compared with their coarse grained counterparts. Reasonable ductility in ultrafine grained steel can be attributed to the presence of finely dispersed particles which improve the work hardening capacity owing to the accumulation of geometrically necessary dislocations around the particles. Ultrafine grained steel exhibits a large Lüders strain because of the relatively low work hardening rate due to rapid dynamic recovery in ultrafine grained steel compared with coarse grained steel. In ultrafine grained steel, the upper shelf energy is rela-

tively low due to the occurrence of delaminations. Some factors such as crystallographic texture and alignment of cementite particles along the ferrite grain boundaries, etc., may promote the formation of delaminations. The lower shelf energy is significantly raised and the ductile-to-brittle transition temperature is reduced in ultrafine grained steel compared to conventional steel. This can be attributed to the joint effect of the small ferrite grain size and the occurrence of delamination, which involves a decrease in the triaxiality of the stress state in the impact test samples of the ultrafine grained steel.

Acknowledgements

The authors would like to express their gratitude for the financial support of the European Coal and Steel Community (ECSC). The support of the Max-Planck-Institut für Eisenforschung in Germany and the sponsors of the Advanced Steel Processing and Products Research Center at the Colorado School of Mines in the USA are gratefully acknowledged.

References

[1] G. Frommeyer, J.A. Jiménez, Metall. Mater. Trans. A 36 (2005) 295.
[2] R.Z. Valiev, A.V. Sergueeva, A.K. Mukherjee, Scripta Mater. 49 (2003) 669.
[3] I.V. Alexandrov, R.Z. Valiev, Scripta Mater. 44 (2001) 1605.
[4] V.V. Stolyarov, Y.T. Zhu, T.C. Lowe, R.K. Islamgaliev, R.Z. Valiev, Nanostruct. Mater. 11 (1999) 947.
[5] R.Z. Valiev, Mater. Sci. Eng. A 234 (1997) 59.
[6] V.M. Segal, Mater. Sci. Eng. A 271 (1999) 322.
[7] Y. Fukuda, K. Oh-Ishi, Z. Horita, T.G. Langdon, Acta Mater. 50 (2002) 1359.
[8] J. Kim, I. Kim, D.H. Shin, Scripta Mater. 45 (2001) 421.
[9] D.H. Shin, I. Kim, J. Kim, K.T. Park, Acta Mater. 49 (2001) 1285.
[10] Z. Horita, M. Furukawa, M. Nemoto, T.G. Langdon, Mater. Sci. Technol. 16 (2000) 1239.
[11] Y.T. Zhu, T.C. Lowe, Mater. Sci. Eng. A 291 (2000) 46.
[12] Y. Saito, H. Utsunomiya, N. Tsuji, T. Sakai, Acta Mater. 47 (1999) 579.
[13] N. Tsuji, R. Ueji, Y. Minamino, Scripta Mater. 47 (2002) 69.
[14] N. Tsuji, Y. Saito, H. Utsunomiya, S. Tanigawa, Scripta Mater. 40 (1999) 795.
[15] T. Inoue, S. Torizuka, K. Nagai, Proceedings of the International Symposium on Ultrafine Grained Steels (ISUGS 2001), The Iron and Steel Institute of Japan, Fukuoka, Japan, 2001, pp. 88–91.
[16] Y. Ivanisenko, R.Z. Valiev, W. Lojkowski, A. Grob, H.J. Fecht, Ultrafine Grained Materials, vol. II, TMS, Seattle, USA, 2002, pp. 47–54.
[17] Y. Ivanisenko, R.K. Wunderlich, R.Z. Valiev, H.J. Fecht, Scripta Mater. 49 (2003) 947.
[18] Y. Ivanisenko, W. Lojkowski, R.Z. Valiev, H.J. Fecht, Acta Mater. 51 (2003) 5555.
[19] R.Z. Valiev, I.V. Alexandrov, Ann. Chim. Sci. Matér. 27 (2002) 3.
[20] V.M. Segal, V.I. Reznikov, A.D. Drobyshevskiy, V.I. Kopylov, Russ. Metall. 1 (1981) 99.
[21] R.Z. Valiev, N.A. Krasilnikov, N.K. Tsenev, Mater. Sci. Eng. A 137 (1991) 35.
[22] D.H. Shin, B.C. Kim, Y.-S. Kim, K.-T. Park, Acta Mater. 48 (2000) 2247.
[23] N. Kamikawa, N. Tsuji, Y. Minamino, Sci. Technol. Adv. Mater. 5 (2004) 163.
[24] N. Tsuji, Y. Ito, Y. Saito, Y. Minamino, Scripta Mater. 47 (2002) 893.
[25] Y. Saito, N. Tsuji, H. Utsunomiya, T. Sakai, R.G. Hong, Scripta Mater. 39 (1998) 1221.
[26] R. Kaspar, J.S. Distl, O. Pawelski, Steel Res. 59 (1988) 421.
[27] P.D. Hodgson, M.R. Hickson, R.K. Gibbs, Scripta Mater. 40 (1999) 1179.
[28] H. Mabuchi, T. Hasegawa, T. Ishikawa, ISIJ Int. 39 (1999) 477.
[29] Z.M. Yang, R.Z. Wang, ISIJ Int. 43 (2003) 761.
[30] J.K. Choi, D.H. Seo, J.S. Lee, K.K. UM, W.Y. Choo, ISIJ Int. 43 (2003) 764.
[31] M.R. Hickson, P.J. Hurley, R.K. Gibbs, G.L. Kelly, P.D. Hodgson, Metall. Mater. Trans. A 33 (2002) 1019.
[32] S.C. Hong, S.H. Lim, K.J. Lee, D.H. Shin, K.S. Lee, ISIJ Int. 43 (2003) 394.
[33] Y. Matsumura, H. Yada, ISIJ Int. 27 (1987) 492.
[34] A. Najafi-Zadeh, J.J. Jonas, S. Yue, Metall. Trans. A 23 (1992) 2607.
[35] N. Tsuji, Y. Matsubara, Y. Saito, Scripta Mater. 37 (1997) 477.
[36] S.V.S. Murty, S. Torizuka, K. Nagai, T. Kitai, Y. Kogo, Scripta Mater. 53 (2005) 763.
[37] J. Baczynski, J.J. Jonas, Metall. Trans. A 29 (1998) 447.
[38] Y. Weng, ISIJ Int. 43 (2003) 1675.
[39] R. Song, D. Ponge, D. Raabe, R. Kaspar, Acta Mater. 53 (2005) 845.
[40] R. Song, R. Kaspar, D. Ponge, D. Raabe, Ultrafine Grained Materials, vol. III, TMS, Charlotte, North Carolina, USA, 2004, p. 445.
[41] R. Song, D. Ponge, R. Kaspar, D. Raabe, Z. Metallkd. 95 (2004) 513.
[42] R. Song, D. Ponge, D. Raabe, Scripta Mater. 52 (2005) 1075.
[43] R. Song, D. Ponge, R. Kaspar, Steel Res. 75 (2004) 33.
[44] R. Song, D. Ponge, D. Raabe, Acta Mater. 53 (2005) 4881.
[45] R. Song, D. Ponge, D. Raabe, ISIJ Int. 45 (2005) 1721.
[46] Y.I. Son, Y.K. Lee, K.-T. Park, C.S. Lee, D.H. Shin, Acta Mater. 53 (2005) 3125.
[47] G. Azevedo, R. Barbosa, E.V. Pereloma, D.B. Santos, Mater. Sci. Eng. A 402 (2005) 98.
[48] K.-T. Park, S.Y. Han, B.D. Ahn, D.H. Shin, Y.K. Lee, K.K. Um, Scripta Mater. 51 (2004) 909.
[49] R. Ueji, N. Tsuji, Y. Minamino, Y. Koizumi, Acta Mater. 50 (2002) 4177.
[50] N. Tsuji, R. Ueji, Y. Minamino, Y. Saito, Scripta Mater. 46 (2002) 305.
[51] R. Ueji, N. Tsuji, Y. Minamino, Y. Koizumi, Sci. Technol. Adv. Mater. 5 (2004) 153.
[52] M.R. Hickson, P.D. Hodgson, Mater. Sci. Technol. 15 (1999) 85.
[53] P.J. Hurley, P.D. Hodgson, B.C. Muddle, Scripta Mater. 40 (1999) 433.
[54] P.J. Hurley, P.D. Hodgson, Mater. Sci. Eng. A 302 (2001) 206.
[55] H. Mabuchi, T. Hasegawa, T. Ishikawa, ISIJ Int. 39 (1999) 477.
[56] R. Priestner, A.K. Ibraheem, Mater. Sci. Technol. 16 (2000) 1267.
[57] H. Yada, Y. Matsumura, K. Nakajima, United State Patent, 4,466,842, Nippon Steel Corporation, Tokyo (1984).
[58] D.J. Hamre, D.K. Matlock, J.G. Speer, in: E. Essadiqi, J. Thomson (Eds.), Ultra-fine Structured Steels, Canada Institute of Mining, Metallurgy, and Petroleum, Montreal, Canada, 2004, pp. 109–121.
[59] W.J. Kim, J.K. Kim, W.Y. Choo, S.I. Hong, J.D. Lee, Mater. Lett. 51 (2001) 177.
[60] S. Nanba, M. Nomura, N. Matsukura, K. Makii, Y. Shirota, Proceedings of the International Symposium on Ultrafine Grained Steels (ISUGS 2001), The Iron and Steel Institute of Japan, Fukuoka, Japan, 2001, pp. 286–289.
[61] H.J. McQueen, N.D. Ryan, in: E. Essadiqi, J. Thomson (Eds.), Ultra-fine Structured Steels, Met. Soc. CIM, 2004, pp. 55–67.
[62] D.H. Shin, B.C. Kim, K.-T. Park, W.Y. Choo, Acta Mater. 48 (2000) 3245.
[63] K.-T. Park, Y.K. Lee, D.H. Shin, ISIJ Int. 45 (2005) 750.
[64] N. Tsuji, Y. Saito, S.-H. Lee, Y. Minamino, Adv. Eng. Mater. 5 (2003) 338.
[65] X. Huang, N. Tsuji, N. Hansen, Y. Minamino, Mater. Sci. Eng. A 340 (2003) 265.
[66] M. Hölscher, D. Raabe, K. Lücke, Steel Res. 62 (1991) 567.
[67] M. Hölscher, D. Raabe, K. Lücke, Acta Metall. 42 (1994) 879.
[68] D. Raabe, K. Lücke, Mater. Sci. Technol. 9 (1993) 302.
[69] D. Raabe, Mater. Sci. Technol. 11 (1995) 461.
[70] M.R. Hickson, R.K. Gibbs, P.D. Hodgson, ISIJ Int. 39 (1999) 1176.
[71] Z.M. Yang, R.Z. Wang, ISIJ Int. 43 (2003) 761.
[72] J.-K. Choi, D.-H. Seo, J.-S. Lee, K.-K. Um, W.-Y. Choo, ISIJ Int. 43 (2003) 746.
[73] P.J. Hurley, G.L. Kelly, P.D. Hodgson, Mater. Sci. Technol. 16 (2000) 1273.

[74] S.C. Hong, S.H. Lim, K.J. Lee, D.H. Shin, K.S. Lee, ISIJ Int. 43 (2003) 394.
[75] S.C. Hong, K.S. Lee, Mater. Sci. Eng. A 323 (2002) 148.
[76] A. Bodin, J. Sietsma, S. van der Zwaag, Mater. Charact. 47 (2001) 187.
[77] G.H. Akbari, C.M. Sellars, J.A. Whiteman, Acta Mater. 45 (1997) 5047.
[78] D.H. Shin, J.-J. Park, S.Y. Chang, Y.-K. Lee, K.-T. Park, ISIJ Int. 42 (2002) 1490.
[79] D.H. Shin, C.W. Seo, J. Kim, K.-T. Park, W.Y. Choo, Scripta Mater. 42 (2000) 695.
[80] M.Y. Liu, B. Shi, C. Wang, S.K. Ji, X. Cai, H.W. Song, Mater. Lett. 57 (2003) 2798.
[81] R. Song, Microstructure and Mechanical Properties of Ultrafine Grained C–Mn Steels, Shaker Verlag GmbH, Aachen, 2005, p. 126.
[82] W.B. Morrison, Trans. ASM 59 (1966) 824.
[83] A.A.W. Thompson, Acta Metall. 23 (1975) 1337.
[84] A.A.W. Thompson, Acta Metall. 25 (1977) 83.
[85] W.M. Baldwin, Acta Metall. 6 (1958) 139.
[86] R.W. Armstrong, I. Codd, R.M. Douthwaite, N.J. Petch, Philos. Mag. 7 (1962) 45.
[87] J.D. Campbell, K.J. Marsh, Philos. Mag. 7 (1962) 933.
[88] H. Conrad, Acta Metall. 11 (1963) 75.
[89] N.J. Petch, Iron Steel Inst. 174 (1953) 25.
[90] A.H. Cottrell, Trans. Metall. Soc. AIME 212 (1958) 192.
[91] J.S. Koehler, Phys. Rev. 85 (1952) 480.
[92] A.A. Johnson, Philos. Mag. 7 (1962) 177.
[93] H. Conrad, S. Feuerstein, L. Rice, Mater. Sci. Eng. 2 (1967) 157.
[94] J.C.M. Li, Trans. Metall. Soc. AIME 227 (1963) 239.
[95] J.C.M. Li, Y.T. Chou, Metall. Trans. 1 (1970) 1145.
[96] C.S. Pande, R.A. Masumura, R.W. Armstrong, Nanostruct. Mater. 2 (1993) 323.
[97] J.D. Eshelby, F.C. Frank, Philos. Mag. 42 (1951) 351.
[98] T.E. Mitchell, S.S. Hecker, R.L. Smialek, Phys. Stat. Sol. 11 (1965) 585.
[99] R.W. Armstrong, Y.T. Chou, R.M. Fisher, N. Louat, Philos. Mag. 14 (1966) 943.
[100] H.W. Song, S.R. Guo, Z.Q. Hu, Nanostruct. Mater. 11 (1999) 203.
[101] M. Liu, B. Shi, G. Bi, H. Cao, X. Cai, H. Song, Mater. Sci. Eng. A 360 (2003) 101.
[102] K.T. Park, Y.S. Kim, J.G. Lee, D.H. Shin, Mater. Sci. Eng. A 293 (2000) 165.
[103] A. Azushima, K. Aoki, Mater. Sci. Eng. A 337 (2002) 45.
[104] K.-T. Park, S.Y. Han, D.H. Shin, Y.-K. Lee, K.J. Lee, K.S. Lee, ISIJ Int. 44 (2004) 1057.
[105] T. Hanamura, F. Yin, K. Nagai, ISIJ Int. 44 (2004) 610.
[106] R.Z. Valiev, E.V. Kozlov, Y.F. Ivanov, J. Lian, A.A. Nazarov, B. Baudelet, Acta Metall. Mater. 42 (1994) 2467.
[107] J. Lian, B. Baudelet, A.A. Nazarov, Mater. Sci. Eng. A 172 (1993) 23.
[108] W. Lojkowski, Acta Metall. Mater. 39 (1991) 1891.
[109] R.E. Reed-Hill, R. Abbaschian, Physical Metall Principles, PWS Publishing Company, 1994, p. 158.
[110] M.F. Ashby, Philos. Mag. 21 (1970) 399.
[111] J.C. Fisher, E.W. Hart, R.H. Pry, Acta Mater. 1 (1953) 336.
[112] A.A. Howe, Mater. Sci. Technol. 16 (2000) 1264.
[113] D.J. Lloyd, L.R. Morris, Acta Metall. 25 (1977) 857.
[114] J.S. Hayes, R. Keyte, P.B. Prangnell, Mater. Sci. Technol. 16 (2000) 1259.
[115] Z.C. Wang, P.B. Prangnell, Mater. Sci. Eng. A 328 (2002) 87.
[116] N. Tsuji, S. Okuno, Y. Koizumi, Y. Minamino, Mater. Trans. 45 (2004) 2272.
[117] A.L. Sjong, R.L. Bodnar, M.J. Merwin, D.K. Matlock, J.G. Speer, in: R.I. Asfahani, R.L. Bodnar, M.J. Merwin (Eds.), Proceedings of the Symposium on Microalloyed Steels, Ohio, 2002, pp. 92–100.
[118] R. Kaspar, H. Faul, MP Materialprüfung 43 (2001) 18.
[119] S. Kim, Y.R. Im, S. Lee, H.C. Lee, Y.J. Oh, J.H. Hong, Metall. Mater. Trans. A: Phys. Metall. Mater. Sci. 32 (2001) 903.
[120] P. Brozzo, G. Buzzichelli, A. Mascanzoni, M. Mirabile, Met. Sci. 11 (1977) 123.
[121] B.L. Bramfitt, A.R. Marder, Metall. Trans. A 8 (1977) 1263.
[122] T. Hashimoto, T. Sawamura, H. Ohtani, Iron Steel Inst. Jpn. 65 (1979) 1425.
[123] S. Matsuda, Y. Kawashima, S. Sekiguchi, M. Okamoto, Iron Steel Inst. Jpn. 68 (1982) 436.
[124] A. Ohmori, S. Torizuka, K. Nagai, Iron Steel Inst. Jpn. 89 (2003) 765.
[125] P. Shanmugam, S.D. Pathak, Eng. Fract. Mech. 53 (1996) 991.
[126] R. Schofield, G. Roentree, N.V. Sarma, R.T. Weiner, Met. Technol. (1974) 325.
[127] A.J. McEvely, R.H. Rush, Trans. ASM 55 (1962) 654.
[128] E. Miyoshi, M. Fukuda, H. Iwanaga, Okazawa T, Proceedings of the Inst. of Gas Eng. Conference, 1974 (paper 4).
[129] W. Pitsch, G. Sauthoff, H.P. Hougardy, in: V.D. Eisenhüttenleute (Ed.), A Handbook for Mater Research and Engineering, vol. 1, Springer-Verlag, 1992, p. 278.
[130] M. Fujioka, T. Yokota, Y. Adachi, N. Matsukura, Proceedings of the Second Symposium on Super Metal, Japan, 1999, p. 193.
[131] K. Nagai, Mater. Proc. Technol. 117 (2001) 329.